Performance of TES X-Ray Microcalorimeters Designed for 14.4-keV Solar Axion Search

Y. Yagi[1,3] · R. Konno[1,4] · T. Hayashi[2] · K. Tanaka[1,3] · N. Y. Yamasaki[1,3,4] ·
K. Mitsuda[5] · R. Sato[6] · M. Saito[7] · T. Homma[6,7] · Y. Nishida[8] · S. Mori[8] ·
N. Iyomoto[8] · T. Hara[9]

Abstract

A ^{57}Fe nucleus in the solar core could emit a 14.4-keV monochromatic axion through the M1 transition if a hypothetical elementary particle, axion, exists to solve the strong CP problem. Transition edge sensor (TES) X-ray microcalorimeters can detect such axions very efficiently if they are again converted into photons by a ^{57}Fe absorber. We have designed and produced a dedicated TES array with ^{57}Fe absorbers for the solar axion search. The iron absorber is set next to the TES, keeping a certain distance to reduce the iron-magnetization effect on the spectroscopic performance. A gold thermal transfer strap connects them. A sample pixel irradiated from a ^{55}Fe source detected 698 pulses. In contrast to thermal simulations, we consider that the pulses include either events produced in an iron absorber or gold strap at a fraction dependent on the absorption rate of each material. Furthermore, photons deposited on the iron absorber are detected through the strap as intended. The identification of all events still needs to be completed. However, we successfully operated the TES with the unique design under iron magnetization for the first time.

Keywords Sensors · Microcalorimeters · TES · Solar axions · Monochromatic axion · ^{57}Fe

1 Introduction of Solar Axion Search and TES Detection Sensitivity

An axion is a hypothetical elementary particle proposed to solve the strong CP problem in quantum chromodynamics [1–4]. The axion is one of the dark matter candidates required in the current cosmology. The axion can convert to a photon or vice versa in a certain probability via the axion–photon coupling in an external electric or magnetic field. At the center of the Sun, photons of $kT \sim 1.3$ keV [5] could produce

✉ Y. Yagi
yagi@ac.jaxa.jp

Extended author information available on the last page of the article

axions by the interaction with the magnetic field, and their energy spectrum traces the blackbody radiation [6, 7]. In addition to this process, magnetic dipole (M1) transitions of some nuclei, which can be excited thermally, could also produce axions via the axion–nucleon coupling. ^{57}Fe nuclei have an M1 transition level of 14.4 keV, and Moriyama [8] calculated the monochromatic axion flux from the Sun at 14.4 keV. These monochromatic axions would excite the same ^{57}Fe nuclei in a laboratory on the Earth and would be reconverted to 14.4 keV photons. Moriyama [8] also proposed to search for solar axions by detecting these photons. Moreover, this method has the advantage that the detector does not need to be tuned to the axion mass, unlike dark-matter axion searches.

A silicon-based semiconductor detector searched the 14.4 keV photons from ^{57}Fe film [9–13], and the best upper limit on axion mass of $m_a < 145$ eV [13] is obtained at 95% confidence limit in the KSVZ hadronic axion model [14, 15]. Other experiments using a proportional gas chamber to detect 9.4 keV photons from ^{83}Kr gas bounded on the hadronic axion mass of $m_a < 12.7$ eV (95% C.L.) [16, 17]. In the ^{57}Fe film experiment, the branching ratio to emit a 14.4-keV photon is only 10.5%, and the rest are converted to electrons or low-energy X-rays. Moreover, the iron film itself absorbs about 80% of the photons. The combination of an iron film and any silicon-based detectors was not able to detect the self-absorbed thermal energy from axions in the film. Therefore, the detection efficiency was not more than 10%. We came up with the idea that a transition edge sensor (TES) X-ray microcalorimeter array with ^{57}Fe absorbers could be a solar axion detector. This is because the microcalorimeters can detect not only 14.4 keV photons but also all dissipated energy in the absorbers. Also, the excellent energy resolution of TES microcalorimeters would improve the sensitivity for the monochromatic axions, with enough converter mass and exposure time.

We assume a ^{57}Fe axion converter size of $100 \times 100 \times 10\ \mu m^3$ and an iron density of 7.874 g/cm^3. The on-ground background rate of the X-ray spectrometer (XRS) for *Suzaku* observatory using the anti-coincidence detector was 2.0×10^{-3} counts/s/cm^2/keV [18]. We conservatively expect the background rate of 1.0×10^{-2} counts/s/cm^2/keV. Our group achieved the full width at half maximum (FWHM) energy resolution of $14.41^{+5.05}_{-4.03}$ eV at 13.94 keV [19] and successfully fabricated a 64-pixel TES array [20]. Figure 1 shows the estimated 3σ detection limits against the number of pixels (i.e., axion converter mass), with various energy resolutions and exposure times. A detection limit can be converted into an axion mass limit with Eq. 3 and 7 in [8]. Here, parameter values of $D = 0.808$, $F = 0.462$, $S = 0.5$, and $z = 0.56$ in the hadronic axion [21] are used. As a simultaneous readout of 38 TES pixels via microwave multiplex (MWMUX) readout system [22] has been demonstrated [23, 24], the production of a extensive format array system is promising with our technologies.

2 Microcalorimeter Design and Fabrication

The energy resolution of TES could degrade if it is operated under a magnetic field made by a ferromagnetic iron absorber. The effect depends on the direction of the field through a TES [25]. The perpendicular magnetic field affects badly,

Fig. 1 The 3σ detection limits as a function of the number of pixels whose ^{57}Fe absorber size is $100 \times 100 \times 10\ \mu m^3$. The exposure time for more than 100 days using a 256-pixel TES array with less than 15 eV energy resolution exceeds the sensitivity of Namba [11]. More than a ten thousand-pixel array can search for the axion mass range much less than 145 eV in Derbin et al. [13]. (Color figure online)
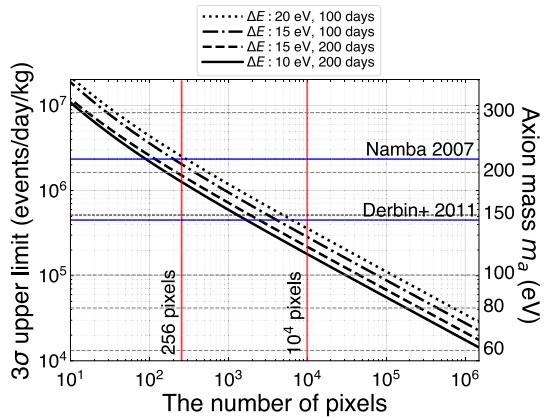
but the horizontal field does not. In order to reduce the magnetic field on the TES, we located the iron absorber next to the TES and connected them with a gold thermal transfer strap, as shown in Fig. 2. We have estimated that the magnetic field becomes less than 1 µT, where we were able to operate TES microcalorimeters without trouble if the distance from the edge of a 5 µm-thickness iron is more than 30 µm [26]. Konno et al. [26] showed the possible degradation of energy resolution, from 10 eV to 32 eV, by the position dependence in the iron absorber under the condition where the conductivity of iron and that of gold are 6.3×10^{-2} and 3.7×10^{-2} W/K/m at 4 K, respectively. Large enough thermal conductivities of both iron and gold are required.
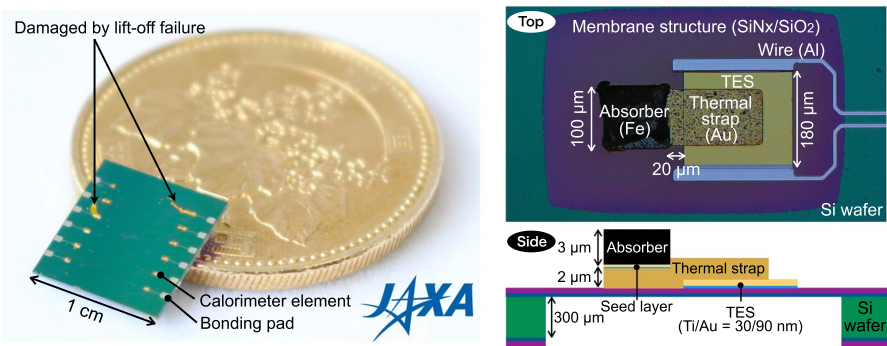

Fig. 2 (*Left*) Our fabricated chip with 12 elements with a Japanese 500-yen coin. It has various distances, 0, 20, 60, 100, 200, 300, and 500 µm, between the iron absorber edge and the TES edge to avoid the magnetic field from the iron absorber. Some elements are damaged due to a failure of the lift-off process of seed layers. (*Right*) A top view of a single-pixel TES microcalorimeter, a sample element used in the irradiation test in Sect. 4, and a side view of its schematic structure. The size of the TES, iron absorber, and membrane structure are $180 \times 180\ \mu m^2$, $100 \times 100\ \mu m^2$, and $300 \times 460\ \mu m^2$, respectively, and the thickness of the absorber, thermal strap, and TES (Ti/Au) are 3 µm, 2 µm, and 30/90 nm, respectively. The distance between the TES and the iron absorber is 20 µm. (Color figure online)

To form thick iron absorbers, we have been developing a recipe for electroplating pure iron in the facilities of the Nanotechnology Research Center (NTRC) at Waseda University. Electroplating is very effective method to produce a small structure with expensive materials like a ^{57}Fe isotope. Although we need a high density and good thermal conductivity in the absorber, pure iron is rarely used commercially, and thus, standard process has not yet been established. We made several test samples by reacting in an iron-liquid solution of not expensive normal ^{56}Fe. We measured electric resistances at room temperature and 4 K using the LR-700 AC resistance bridge of Linear Research Inc. We achieved effective deposition even in low solution concentration, 0.05 mol/L, after adjusting the electric current, the time, and additions in the solution. The thermal conductivities, 2.0–5.4 W/K/m at 4 K, calculated from the Wiedemann–Franz law, were more than 30 times higher and more efficient heat transmission than the former worst case value, 6.3×10^{-2} W/K/m, used in the estimation of the degradation by position dependence [26].

We fabricated a test device of this newly designed TES microcalorimeter in the nanoelectronics clean room at ISAS/JAXA in a process flow shown in Fig. 3. Firstly, proximity-coupled titanium/gold TES bilayer was deposited by sputtering, and aluminum leads were attached. Secondly, gold thermal transfer straps of 2 µm thickness were evaporated by the electron beam physical vapor deposition. Thirdly, iron absorbers of 3 µm thickness were electroplated on the electrode seed layer. Then, the film was electroplated twice because the target thickness was not reached the first time. The device has various distances, 0, 20, 60, 100, 200, 300, and 500 µm, between an iron-absorber edge and a TES edge to avoid the magnetic field from the iron absorber. Finally, membrane structures of SiN_x /SiO_2 under TES were formed by a deep reactive ion etching. Sixteen pixels out of twenty-four were successfully produced, as shown in Fig. 2. We have not yet established the fabrication process completely. Some photoresist compositions remained and made wrinkles after iron electrodeposition in Fig. 3. The lift-off of the seed layers failed in some pixels in Fig. 2, *left*. We suspect that the rough gold surface, due to the high deposition rate, caused an adhesion reduction with the seed layer on the straps.
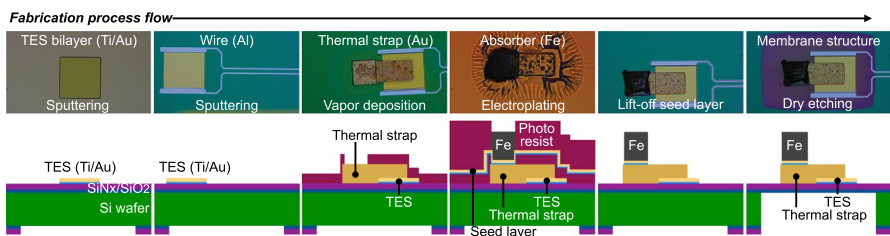

Fig. 3 Our fabrication process flow of the TES microcalorimeter placed with a distance between the iron absorber and the TES. (Color figure online)

3 Non-uniformity of Iron Absorber and Investigation by Material Analysis

We observed the fabricated chips and found unexpected black materials from the back in all elements after membrane structure formation, as shown in Fig. 4a. As the iron surface was rough and curled, we suspected that the irons, designed only on gold thermal straps, were deposited wrongly. For analyzing these materials, an element was vertically cut with a focused ion beam (FIB) (Fig. 4b), and we observed the cross-section by the scanning electron microscope (SEM) and energy-dispersive X-ray spectroscopy (EDS) (Fig. 4c–e). These images indicate that the iron and the seed layer curled up together due to the iron tensile stress in an early phase of the first electroplating, and then, the gold strap was also peeled off partially from the wafer. In the second electroplating, the iron structures were deposited under the seed layer and on and under the gold strap. Although the size of the gold strap has a 5 µm extra margin to the iron size not to protrude from the strap, if the photolithographic pattern on the strap is out of alignment by more than the margin, a gap between a photoresist and a strap edge occurs. Therefore, the iron solution could encroach on the back of the gold straps from the gap. This hypothesis indicates that more accurate pattering or designing the larger strap area than the iron absorber is favored. Also, to increase the adhesion between the seed layer and the strap, a new gold electroplating process for straps is under testing to fabricate smoother surfaces. In general, the electroplating makes 10 times higher thermal conductivity at 4 K compared to the vapor deposition we used this time. The residual resistance ratio (RRR) of 300 K to 4 K is around 30 [27].

4 X-Ray Irradiation Test and Pulse Shapes

We performed an X-ray irradiation test under a cryogenic temperature of an iron-absorber–TES microcalorimeter with a 20 µm distance between the absorber and the TES (Fig. 2). Figure 5 shows the measured IV curve at different bath temperatures. An X-ray source (^{55}Fe isotope) and a silicon collimator were mounted above the chip at about 6 mm and 320 µm, respectively. The normal state resistance is 136 mΩ.

Fig. 4 **a** Optical microscopical image of calorimeter back side. **b** FIB processing position seen from the front. This element has a 200 µm distance from the iron to the TES. **c** The SEM image of the iron surface and the cross-section. **d** Fe-L EDS map. The iron membrane was deposited under the gold strap, not only on it. **e** Au-M EDS map. The iron membrane and the seed layer curled up together. (Color figure online)
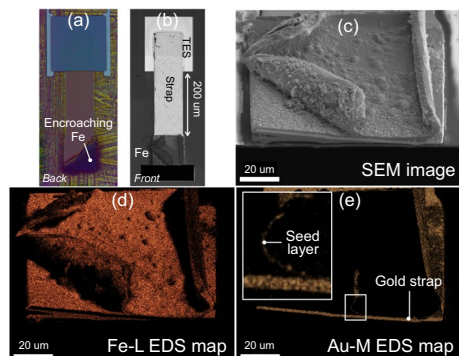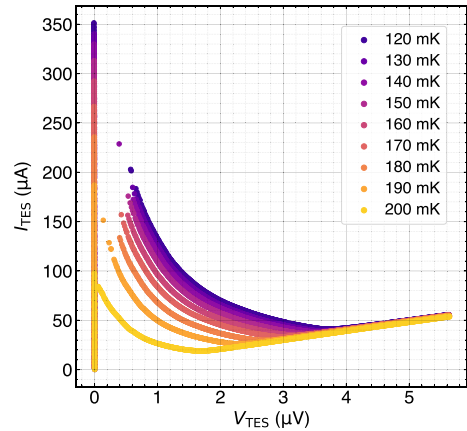
Fig. 5 Corrected IV, current and voltage, the curve of the TES with a 20 µm distance from the iron absorber at different bath temperatures. (Color figure online)

The transition temperature was 214 mK, and the operating temperature was set to 130 mK. The α ($= d \ln R / d \ln T$) is around 100. The TES was connected to a superconducting quantum interference device (SQUID) amplifier and operated under a standard electrothermal feedback (ETF) method.

In about three days, 698 waveforms of signal pulses were recorded with a time resolution of 24 ns. The pulse shapes were not identical or similar. These were divided into two types. "Normal"-type pulses are characterized by their rising time in the order between microseconds and milliseconds and by the falling time in a few milliseconds. Others are called "Spike"-type pulses because a few microseconds fast spike is seen at the beginning of the pulses, followed by a slow falling time in about a millisecond. The pulse events were classified into nine groups by their pulse shapes, and averaged pulses in each group are shown in Fig. 6. The number of pulses, rising time τ_{rise}, and falling time τ_{fall} in each group are given in Table 1. X-ray radiation spread over the vicinity of the iron absorber, including the thermal strap and TES area, because the collimator was not small enough compared to the distance from the chip. Consequently, X-rays could deposit at the absorber, thermal strap, TES, and membrane and make signal pulses with different time scales. We are working on reproducing obtained pulse shapes with a realistic thermal model using a finite element method with COMSOL Multiphysics software [28] to identify the event location by pulse shapes. According to the simulation, the iron absorber and
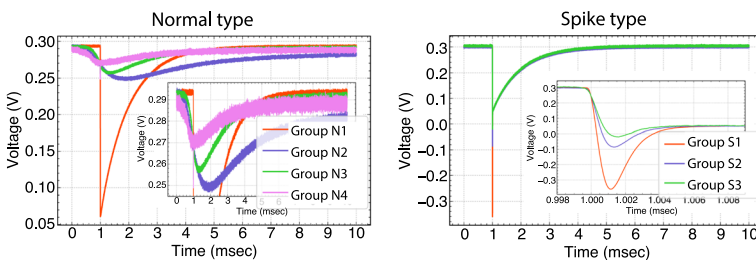

Fig. 6 The average pulses in each group classified by shape. (Color figure online)

Table 1 The number of pulses, rising time τ_{rise}, and falling time τ_{fall} in each group

Pulse type	Normal type					Spike type			
Group	N1	N2	N3	N4	The others	S1	S2	S3	The others
Number	151	57	117	20	33	206	80	18	16
τ_{rise} (µs)	0.40–1.7	4.0×10^2	$(1.0–3.0)\times10^2$	$(1.3–2.5)\times10^3$	–	0.70–0.90	1.0–1.2	1.2–1.4	–
τ_{fall} (ms)	0.80–0.90	4.0–5.3	1.2–2.2	0.10–0.30	–	0.80–1.0	0.90–1.0	0.90–1.0	–

In the spike type, τ_{fall} is the second slow falling time

the thermal strap events have similar pulse shapes. Regardless of absorbing positions in the absorber or strap, events up to about 50 µm far from the TES edge have a spike shape, and events farther than that have a normal shape. The falling times of both shapes are 0.47 ms. In either of the pulse shapes, the rise time of absorber events is about 0.5–2.7µs and is faster and closer to the TES. On the other hand, the thermal strap events under Fe are about the same, and the events closer to TES have an even faster rising time. They are comparable with Groups N1 and S in Table 1. Therefore, the obtained data include both the iron absorber and gold strap events at a fraction dependent on the absorption rate of each material. As intended, the X-ray photons deposited on the iron absorber are detected through the thermal strap.

5 Conclusion and Future Prospects

We successfully deposited iron absorbers whose thermal conductivities are 2.0–5.4 W/K/m at 4 K using ^{56}Fe and produced the first test calorimeters for the solar axion detector. In irradiation tests, it was likely that iron events were detected. The identification of all events still needs to be completed. However, for the first time, we successfully operated the TES microcalorimeter with a certain distance between the iron absorber and the TES under iron magnetization. The high thermal conductivity of gold thermal straps could decrease the effect of degrading the energy resolution by the position dependence in an absorber discussed in [26]. To make efficient detectors, we try to deposit gold straps by electroplating and continue to fabricate iron absorbers with high conductivity.

References

1. R.D. Peccei, H.R. Quinn, Phys. Rev. Lett. **38**, 1440 (1977). https://doi.org/10.1103/PhysRevLett.38.1440

2. R.D. Peccei, H.R. Quinn, Phys. Rev. D **16**, 1791 (1977). https://doi.org/10.1103/PhysRevD.16.1791
3. S. Weinberg, Phys. Rev. Lett. **40**, 223 (1978). https://doi.org/10.1103/PhysRevLett.40.223
4. F. Wilczek, Phys. Rev. Lett. **40**, 279 (1978). https://doi.org/10.1103/PhysRevLett.40.279
5. S. Turck-Chiéze, W. Däppen, E. Fossat, J. Provost, E. Schatzman, D. Vignaud, Phys. Rep. **230**, 57 (1993). https://doi.org/10.1016/0370-1573(93)90020-E
6. K. van Bibber, P.M. McIntyre, D.E. Morris, G.G. Raffelt, Phys. Rev. D **39**, 2089 (1989). https://doi.org/10.1103/PhysRevD.39.2089
7. F. Hoogenveen, R.G. Stuart, Phys. Lett. B **286**, 165 (1992). https://doi.org/10.1016/0370-2693(92)90175-4
8. S. Moriyama, Phys. Rev. Lett. **75**, 3222 (1995). https://doi.org/10.1103/PhysRevLett.75.3222
9. M. Krčmar, Z. Krečak, M. Stipčević, A. Ljubičić, andD. A. Bradley *Phys. Lett. B* **442**, 38 (1998), https://doi.org/10.1016/S0370-2693(98)01231-3
10. A.V. Derbin, A.I. Egorov, I.A. Mitropol'sky, V.N. Muratova, N.V. Bazlov, S.V. Bakhlanov, D.A. Semenov, E.V. Unzhakov, JETP Lett. **85**, 12 (2007). https://doi.org/10.1134/S0021364007010031
11. T. Namba, Phys. Lett. B **645**, 398 (2007). https://doi.org/10.1016/j.physletb.2007.01.005
12. A.V. Derbin, A.I. Egorov, I.A. Mitropolsky, V.N. Muratova, D.A. Semenov, E.V. Unzhakov, Eur. Phys. J. C **62**, 755 (2009). https://doi.org/10.1140/epjc/s10052-009-1095-y
13. A.V. Derbin, V.N. Muratova, D.A. Semenov, E.V. Unzhakov, Phys. Atom. Nucl. **74**, 596 (2011). https://doi.org/10.1134/S1063778811040041
14. J.E. Kim, Phys. Rev. Lett. **43**, 103 (1979). https://doi.org/10.1103/PhysRevLett.43.103
15. M.A. Shifman, A.I. Vainshtein, V.I. Zakharov, Nucl. Phys. B **166**, 493 (1980). https://doi.org/10.1016/0550-3213(80)90209-6
16. Y.M. Gavrilyuk, A.N. Gangapshev, A.V. Derbin, I.S. Drachnev, V.V. Kazalov, V.V. Kobychev, V.V. Kuz'minov, V.N. Muratova, S.I. Panasenko, S.S. Ratkevich, D.A. Semenov, D.A. Tekueva, E.V. Unzhakov, S.P. Yakimenko, JETP Lett. **101**, 664 (2015). https://doi.org/10.1134/S0021364015100069
17. Y.M. Gavrilyuk, A.N. Gangapshev, A.V. Derbin, I.S. Drachnev, V.V. Kazalov, V.V. Kobychev, V.V. Kuzminov, V.N. Muratova, S.I. Panasenko, S.S. Ratkevich, D.A. Tekueva, E.V. Unzhakov, S.P. Yakimenko, JETP Lett. **107**, 589 (2018). https://doi.org/10.1134/S0021364018100090
18. R. L. Kelley, K. Mitsuda, C. A. Allen, P. Arsenovic, M. D. Audley, T. G. Bialas, K. R. Boyce, R. F. Boyle, S. R. Breon, G. V. Brown, J. Cottam, M. J. Di Pirro, R. Fujimoto, T. Furusho, K. C. Gendreau, G. G. Gochar, O. Gonzalez, M. Hirabayashi, S. S. Holt, Hajime Inoue, Manabu Ishida, Y. Ishisaki, C. S. Jones, R. Keski-Kuha, C. A. Kilbourne, D. McCammon, U. Morita, S. H. Moseley, B. Mott, K. Narasaki, Y. Ogawara, T. Ohashi, N. Ota, J. S. Panek, F. S. Porter, A. Serlemitsos, P. J. Shirron, G. A. Sneiderman, A. E. Szymkowiak, Y. Takei, J. L. Tveekrem, S. M. Volz, M. Yamamoto, and N. Y. Yamasaki, *Publ. Astron. Soc. Jpn.* **59**, 77, (2007), https://doi.org/10.1093/pasj/59.sp1.S77.
19. H. Muramatsu, T. Hayashi, K. Maehisa, Y. Nakashima, K. Mitsuda, N.Y. Yamasaki, T. Hara, K. Maehata, IEEE Trans. Appl. Supercond. **27**, 1 (2017). https://doi.org/10.1109/TASC.2017.2661738
20. H. Muramatsu, K. Nagayoshi, T. Hayashi, K. Sakai, R. Yamamoto, K. Mitsuda, N.Y. Yamasaki, K. Maehata, T. Hara, J. Low Temp. Phys. **184**, 91 (2016). https://doi.org/10.1007/s10909-016-1547-3
21. V. Mateu, A. Pich, J. High Energy Phys. **10**, 41 (2005)
22. J.A.B. Mates, G.C. Hilton, K.D. Irwin, L.R. Vale, K.W. Lehnert, Appl. Phys. Lett. **92**, 023514 (2008). https://doi.org/10.1063/1.2803852
23. Y. Nakashima, F. Hirayama, S. Kohjiro, H. Yamamori, S. Nagasawa, A. Sato, N.Y. Yamasaki, K. Mitsuda, IEEE Trans. Appl. Supercond. **29**, 1 (2019). https://doi.org/10.1109/TASC.2019.2905688
24. Y. Nakashima, F. Hirayama, S. Kohjiro, H. Yamamori, S. Nagasawa, A. Sato, S. Yamada, R. Hayakawa, N.Y. Yamasaki, K. Mitsuda, K. Nagayoshi, H. Akamatsu, L. Gottardi, E. Taralli, M.P. Bruijn, M.L. Ridder, J.R. Gao, J.W.A. den Herder, Appl. Phys. Lett. **117**, 122601 (2020). https://doi.org/10.1063/5.0016333
25. Y. Ishisaki, H. Kurabayashi, A. Hoshino, T. Ohashi, T. Yoshino, T. Hagihara, K. Mitsuda, K. Tanaka, J. Low Temp. Phys. **151**, 131 (2008). https://doi.org/10.1007/s10909-007-9628-y
26. R. Konno, K. Maehisa, K. Mitsuda, N.Y. Yamasaki, R. Yamamoto, T. Hayashi, H. Muramatsu, Y. Nakashima, K. Maehata, T. Homma, M. Saito, M. Sugie, R. Sato, J. Low Temp. Phys. **199**, 645 (2020). https://doi.org/10.1007/s10909-019-02257-9
27. K. Nagayoshi, M.L. Ridder, M.P. Bruijn, L. Gottardi, E. Taralli, P. Khosropanah, H. Akamatsu, S. Visser, J.-R. Gao, J. Low Temp. Phys. **199**, 943 (2020). https://doi.org/10.1007/s10909-019-02282-8

28. S. Mori, Y. Nishida, N. Iyomoto, Y. Yagi, R. Konno, T. Hayashi, K. Tanaka, N. Y. Yamasaki, K. Mitsuda, R. Sato, M. Saito, T. Homma, J. Low Temp. Phys. **209**, 518 (2022). https://doi.org/10.1007/s10909-022-02902-w

Authors and Affiliations

Y. Yagi[1,3] [ID] **· R. Konno[1,4] · T. Hayashi[2] · K. Tanaka[1,3] · N. Y. Yamasaki[1,3,4] · K. Mitsuda[5] · R. Sato[6] · M. Saito[7] · T. Homma[6,7] · Y. Nishida[8] · S. Mori[8] · N. Iyomoto[8] · T. Hara[9]**

[1]   Department of Space Astronomy and Astrophysics, Institute of Space and Astronautical Science (ISAS), Japan Aerospace Exploration Agency (JAXA), 3-1-1 Yoshinodai, Chuo-ku, Sagamihara-shi, Kanagawa 252-5210, Japan

[2]   Astromaterials Science Research Group (ASRG), Institute of Space and Astronautical Science (ISAS),Japan Aerospace Exploration Agency (JAXA), 3-1-1 Yoshinodai, Chuo-ku, Sagamihara-shi, Kanagawa 252-5210, Japan

[3]   Department of Physics, School of Science, The University of Tokyo, 7-3-1 Hongo, Bunkyo-ku, Tokyo 113-0033, Japan

[4]   Department of Physics, School of Science, Kitasato University, 1-15-1 Kitasato, Minami-ku, Sagamihara-shi, Kanagawa 252-0373, Japan

[5]   National Astronomical Observatory of Japan (NAOJ), 2-21-1 Osawa, Mitaka-shi, Tokyo 181-8588, Japan

[6]   Department of Applied Chemistry, School of Advanced Science and Engineering, Waseda University, Okubo 3-4-1, Shinjuku-ku, Tokyo 169-8555, Japan

[7]   Research Organization for Nano and Life Innovation, Waseda University, 513 Waseda-tsurumaki-cho, Shinjuku-ku, Tokyo 162-0041, Japan

[8]   Department of Applied Quantum Physics and Nuclear Engineering, Kyushu University, Motooka 744, Nishi-ku, Fukuoka 819-0395, Japan

[9]   Research Network and Facility Services Division, National Institute for Materials Science (NIMS), 1-2-1 Sengen, Tsukuba, Ibaraki 305-0047, Japan